Available online at www.sciencedirect.com
ScienceDirect
Icarus 195 (2008) 277–294
ICARUS
www.elsevier.com/locate/icarus

Mineralogical analysis of the Eos family from near-infrared spectra

T. Mothé-Diniz [a,b,*], J.M. Carvano [a,b], S.J. Bus [c], R. Duffard [d], T.H. Burbine [e]

[a] *LESIA, Observatoire de Paris, 92195 Meudon, France*
[b] *COAA, Observatório Nacional, Rua Gal. José Cristino, 77, São Cristóvão, 20921-400 Rio de Janeiro, Brazil*
[c] *Institute for Astronomy, University of Hawaii at Hilo, Hilo, HI 96720-2700, USA*
[d] *Max Planck Institute for Solar System Research, 37191 Katlenburg-Lindau, Germany*
[e] *Astronomy Department, Mount Holyoke College, South Hadley, MA 01075, USA*

Received 2 January 2007; revised 19 November 2007

Available online 31 December 2007

Abstract

The aim of this work is to analyze the mineralogy of the Eos family, which exhibits considerable taxonomic diversity. Its biggest fragment, (221) Eos has previously been associated, through direct spectral comparisons, with such diverse mineralogies as CV/CO and achondrite meteorites [Burbine, T.H., Binzel, R.P., Bus, S.J., Clark, B.E., 2001. Meteorit. Planet. Sci. 36, 245–253; Mothé-Diniz, T., Carvano, J.M., 2005. Astron. Astrophys. 174, 54–80]. In order to perform such analysis we obtained spectra of 30 family members in the 0.8–2.5 μm range, and used three different methods of mineralogical inference: direct spectral comparison with meteorites, intimate mixing using Hapke's theory, and fitting absorption features with the MGM. Although the direct comparison failed to yield good matches—the best candidates being R-chondrites—both mixing model and MGM analysis suggest that the bulk of the family is dominated by forsteritic ($Fa_{\sim 20}$) olivine, with a minor component of orthopyroxene. This composition can be compatible with what would be expected from the partial differentiation of a parent-body with an original composition similar to ordinary chondrites, which probably formed and differentiated closer to the Sun than the present location of the family. A CK-like composition is also possible, from the inferred mineralogy, as well as from the similarities of the spectra in the NIR.

Keywords: Asteroids, composition; Spectroscopy

1. Introduction

The first attempts of deciphering the mineralogy of minor planets date back to the 1980s. In particular, the Eos family, located in the outer part of the main belt, was first associated with CO/CV anhydrous meteorites (Bell, 1988). In that work, Bell compared the spectrum of Eos in the near-infrared (NIR) (0.33–2.5 μm) with the available meteorite spectral data, and noticed that the spectra and albedo of some Eos family objects were best matched by CV and CO chondrites. Ten years latter, Doressoundiram et al. (1998) reinforced the association of the Eos family with CO/CV chondrites by showing similarities between the spectra of 45 Eos family members and these types of meteorites in the visible range (0.48–0.92 μm). These authors compared the spectra of the family members with the meteorites measured by Gaffey (1976). Recently, Burbine et al. (2001) compared the NIR (0.44–1.65 μm) spectrum of (221) Eos with a number of CO3/CV3 meteorites and the meteorite CO3 Warrenton was found to be the best analog to Eos among the carbonaceous chondrites. However, they did not use the entire meteorite database available in their comparison. By using the entire RELAB database (Pieters and Hiroi, 2004), Mothé-Diniz and Carvano (2005) found that, in the same range spectral used by Burbine et al. (2001), the spectrum of (221) Eos and (653) Berenike (also a member of the Eos dynamical family) were more similar to the anomalous achondrite Divnoe, an olivine-rich meteorite whose parent-body suffered partial melting. This association suggested a completely different thermal history for the parent-body of the Eos family than if a CO/CV composition was assumed.

From the dynamical point of view, the Eos family has recently been analyzed by Vokrouhlický et al. (2006) in an attempt to understand the structure and history of the family

* Corresponding author at: COAA, Observatório Nacional, Rua Gal. José Cristino, 77, São Cristóvão, 20921-400 Rio de Janeiro, Brazil.
E-mail address: thais.mothe@on.br (T. Mothé-Diniz).

0019-1035/$ – see front matter
doi:10.1016/j.icarus.2007.12.005

through modern dynamical tools. Their work suggests that drifting produced by the Yarkovsky effect could inject fragments of the Eos family in the 9/4 and 7/3 resonances. They were also able to constrain the age of the family to 1.3 Gyr, and to determine a number of suspected interlopers in the family, based on their orbital position which was inconsistent with Yarkovsky evolution.

The purpose of this work is to perform a detailed mineralogical analysis of high signal-to-noise visible and near-infrared (VNIR) spectra of members of the Eos dynamical family. To accomplish this goal we analyzed the spectra of 30 Eos family members obtained in the Infrared Telescope Facility (IRTF). A brief description of the physical and orbital characteristics of the Eos family is presented in the next section. In Section 3 we detail the observation reduction procedures, as well as the observational circumstances of each object. In Section 4.1 we search for meteorites spectroscopically similar to our objects. Section 4.2 contains a detailed mineralogical analysis of all objects through the absorption band modified Gaussian model (MGM) (Sunshine and Pieters, 1993). The radiative transfer model of Hapke (1993) was also used to infer the surface mineralogy of some of the objects. The results of this analysis is presented in Section 4.3. In Section 5, we compare the results from the different methods and discuss their significance.

2. Physical and dynamical characteristics of the family

Located at $2.95 \leqslant a_p \leqslant 3.13$, $0.03 \leqslant e_p \leqslant 0.11$ and $0.155 \leqslant \sin(i_p) \leqslant 0.2$, the Eos family accounts for about 4400 members if a cutoff[1] of 55 $\mathrm{m\,s^{-1}}$ is considered (Vokrouhlický et al., 2006), where a_p, e_p and i_p denote respectively the proper orbital elements: semi-major axis, eccentricity and inclination. The biggest fragment of the family, (221) Eos, is ∼104 km in diameter and belongs to the K taxonomic class. The diameter distribution has a median of ∼31 km, and the median albedo is ∼0.15. The size of the parent-body that originated the family is estimated to be 218 km (Tanga et al., 1999).

Ninety-two of the family members have taxonomic classification (Mothé-Diniz et al., 2005), and the family is the only known to present a high "taxonomic inhomogeneity,"[2] with representatives among a wide range of the Bus' classes (Bus and Binzel, 2002): T, D, Ld, Xk, Xc, X, L, S, C and B (Mothé-Diniz et al., 2005). Nevertheless it is quite well distinguished from the background asteroids, which is mostly composed by C-type objects.

3. Observations

The near-infrared spectra of 22 Eos family members were remotely obtained from the Observatory of Paris with the 3.0-m NASA Infrared Telescope Facility (IRTF) equipped with a 1024 × 1024 InSb array spectrograph (SpeX), and located at the Mauna Kea Observatory in Hawaii during three nights, from February 7 to 9, 2005. The other 10 spectra (two of which were also observed in the run of February 2005) were observed in the IRTF with the same configuration in previous years, as shown in Table 1. We have used a 0.8 arcsec slit oriented in the east–west direction. In the low resolution prism-mode, this slit provides a resolution $R \sim 100$, with a spectrum covering the entire interval from 0.8 to 2.5 μm in a single exposure. For the reduction of the data, we followed the standard procedures of flat field correction and sky subtraction. The spectra were then extracted, calibrated in wavelength, and finally each of them was fit with the ATRAN model for telluric absorption features (Lord, 1992). This process is described in detail by Clark et al. (2004a) and Sunshine et al. (2004). Several spectra of solar analog stars were taken during each night. These stars were used to produce normalized reflectance spectra of the asteroids. The final spectra presented in this paper are the averages of all ratios obtained for each object. The error bars are not plotted, but the errors propagated through the reduction are usually less than the scatter in the data. So, we assume that the scatter in the data is the best estimate of the uncertainties of each measurement. Table 1 lists the asteroids, some observational circumstances and physical characteristics for the objects observed, and in Fig. 1 shows the calibrated spectra of all objects.

3.1. Spectral features

As a general characteristic of the observed objects, we can say that all the spectra obtained present a clear absorption band around 1 μm, with a minimum between 1.0 and 1.1 μm. Most of the objects have a negative continuum slope in the wavelength range 1.5–2.5 μm. A weak 2-μm absorption due to pyroxenes can also be seen in the spectrum of a few objects: 633, 669, 1413, 1416, 1903, 2957 and 3469. A more subtle absorption in the same position seems to be present in other spectra also, suggesting a mixture of olivine and pyroxene as a main component in the surface of the Eos family members.

Whenever a visible (VIS) spectrum was available from SMASSII (Bus and Binzel, 2002) or S3OS2 (Lazzaro et al., 2004) for a given object in the family (Table 1), it was joined to its near-infrared (NIR) spectra. The composite visible-NIR (VNIR) spectra have been obtained by requiring that the reflectance of the NIR portion matched the visible spectrum at 0.8 μm. To this end, both spectra were smoothed with a spline fit, and the NIR spectrum was normalized by the ratio of the VIS to the NIR reflectance at 0.8 μm. The resulting spectra were normalized to unity at 0.55 μm by convention. Besides the characteristics described above, the combined spectra of the Eos family members have some additional particularities: (1) a moderately steep reddish slope from 0.5 to 0.75 μm, and (2) a sharp maximum around 0.75–0.8 μm, as can be seen in Fig. 2.

[1] The method used for defining family membership was the hierarchical clustering method (HCM), which requires that all family members are connected by a chain, where each member is attached to its neighbor by less than a limiting distance, called "cut-off."

[2] It is worth to note that most of the families are taxonomically homogeneous, even though most of them show a considerable spectral variability.

Table 1
Physical characteristics, observational dates for NIR spectra and source of the visible spectra for the objects in this study

Asteroid	Name	IRAS albero	Diam.	m_V	Phase angle	Date	Bus class	Source/VisSpec
221	Eos	0.14	103.9	12.3	13.7	08-Oct-2000	K	SMASSII
339	Dorothea	0.24	38.2	14.6	13.3	08-Feb-2005	K	SMASSII
450	Brigitta	0.13	33.3	15.6	19.9	09-Feb-2005	Xk	–
$513_{[1]}$	Centesima	0.09	50.2	15.1	13.3	29-Mar-2001	K	SMASSII
$513_{[2]}$	Centesima	0.09	50.2	14.0	3.4	08-Feb-2005	K	S3OS2
$579_{[1]}$	Sidonia	0.17	85.6	12.9	9.6	20-Feb-2001	K	SMASSII
$579_{[2]}$	Sidonia	0.17	85.6	13.7	18.3	09-Feb-2005	K	S3OS2
590	Tomyris	0.12	39.9	15.1	17.1	08-Feb-2005	T	S3OS2
633	Zelima	0.19	34.4	14.7	5.5	09–10-Feb-2005	S	SMASSII
639	Latona	0.18	71.2	13.6	13.0	08-Feb-2005	S	SMASSI
653	Berenike	0.24	39.2	14.0	15.1	17-Mar-2003	K	SMASSII
661	Cloelia	0.11	48.0	14.6	15.0	16-Mar-2003	K	SMASSII
669	Kypria	0.14	31.8	15.0	5.9	08-Feb-2005	Ld	–
742	Edisona	0.13	45.6	14.8	11.5	16-Mar-2003	K	SMASSII
766	Moguntia	0.16	31.3	15.2	14.9	10-Feb-2005	Ld	–
798	Ruth	0.16	43.2	13.9	6.1	08-Feb-2005	T	S3OS2
1112	Polonia	0.13	35.8	15.6	14.6	10-Feb-2005	T	–
1129	Neujmina	0.12	34.8	14.7	8.9	09–10-Feb-2005	K	–
1148	Rarahu	0.14	33.2	14.9	4.9	29-Mar-2001	K	SMASSII
1186	Turnera	0.29	35.6	14.6	15.1	09-Feb-2005	Sq/T	SMASSII
1364	Safara	–	–	15.3	5.0	09-Feb-2005	Ld	–
1388	Aphrodite	0.13	25.2	14.4	14.8	08-Feb-2005	L	–
1413	Roucarie	0.17	21.4	15.4	11.6	08-Feb-2005	D	–
1416	Renauxa	0.14	28.9	14.8	9.2	08-Feb-2005	D	–
1903	Adzhimushkaj	–	–	15.4	13.7	17-Mar-2003	K	SMASSII
2315	Czechoslovakia	0.17	23.4	15.7	19.5	08-Feb-2005	D	–
2358	Bahner	–	–	15.3	2.4	08-Feb-2005	Xk	–
2443	Tomeileen	0.15	30.8	14.3	3.5	08-Feb-2005	T	
2957	Tatsuo	0.22	25.6	14.8	13.5	04-Sep-2000		SMASSII
3028	Zhangguoxi	0.14	25.6	14.9	4.6	07-May-2002	T	SMASSII
3318	Blixen	–	–	15.3	8.0	09–10-Feb-2005	D	–
3469	Bulgakov	–	–	15.8	5.1	10-Feb-2005	D	–

4. Mineralogy of the family members

To set constraints on the possible composition of the Eos family members we have used three different methods: (1) comparison with meteorites; (2) modified Gaussian model analysis (Sunshine and Pieters, 1998); and (3) mixing model based on the Hapke's (1993) theory of reflectance.

Each method has its own shortcomings. Direct comparison with meteorite spectra have been widely used (Bell, 1988; Burbine et al., 2001; Mothé-Diniz and Carvano, 2005), but the temperature differences between the asteroidal surfaces and the samples measured in the lab, as well as the existence of space weathering effects on the surface of those bodies render the results of such comparisons inaccurate at best (note however that the effects of space weathering should be less severe for darker material—see discussion in Section 5). We use it here for the sake of completeness, since it has been directly involved in the previous inferences of the composition of (221) Eos. The modified Gaussian model in principle can be used to probe quantitatively the presence of any mineral whose spectra present bands due to crystal-field transitions, and can deal with temperature effects. In practice however the limited set of laboratory calibrations presently available restricts its usefulness to mixtures of olivine and pyroxenes (see Section 4.2 for a fuller description of the methods and its limitations). We use it here to infer the compositions of the olivines and pyroxenes from the spectra, as well as their relative abundances.

Finally, radiative transfer methods like Hapke's are in principle the most physically accurate and allow the inclusion in the model of any material for which a laboratory reflectance spectra is available. The caveat here is that there is no way of simulating temperature effects, and all but a few samples had their spectra taken at temperatures comparable to what is expected in the Main Belt. We used this method here mainly as a way of exploring the existing spectroscopic database for best matching materials. It is also important to stress that any process of fitting is in principle subject to the problem of non-unique solutions. The solutions obtained by the MGM are valid only if the initial assumption of which bands are in the mixture were actually correct, and even so the mathematically ill-defined nature of the problem ensures the existence of multiple equally good solutions. The steps taken to minimize those problems are described in Section 4.2. Similarly, the fact that a set of materials produces a good fit to a spectrum when used in a Hapke model does not ensures that those materials are necessarily in the surface of the body—only that they could be. In this sense a failure to fit the spectra with a particular mineral can be more significative than a good fit.

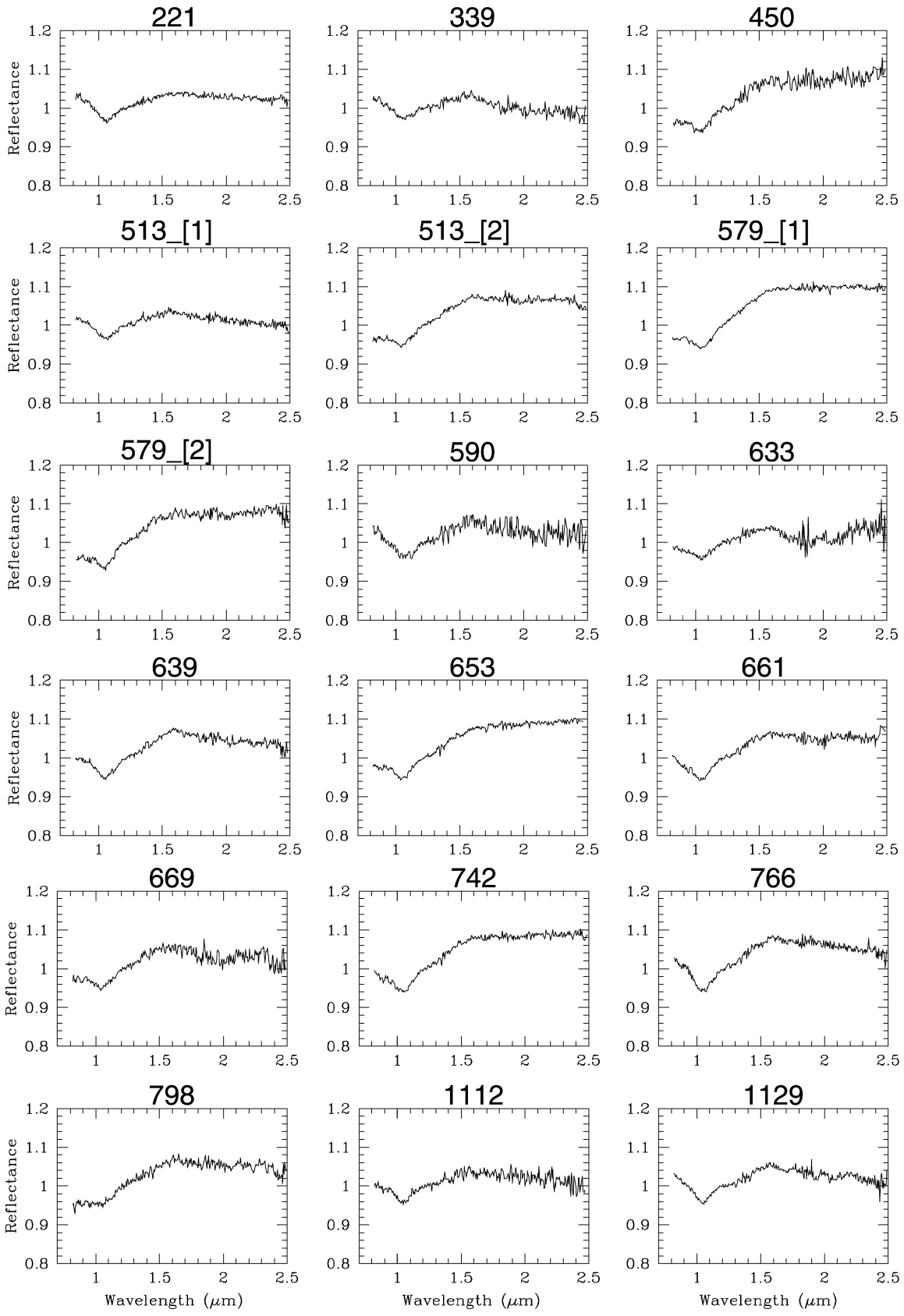

Fig. 1. Reflectance spectra for the 30 Eos family members observed in the IRTF. All spectra are normalized to unity at 1.2 μm.

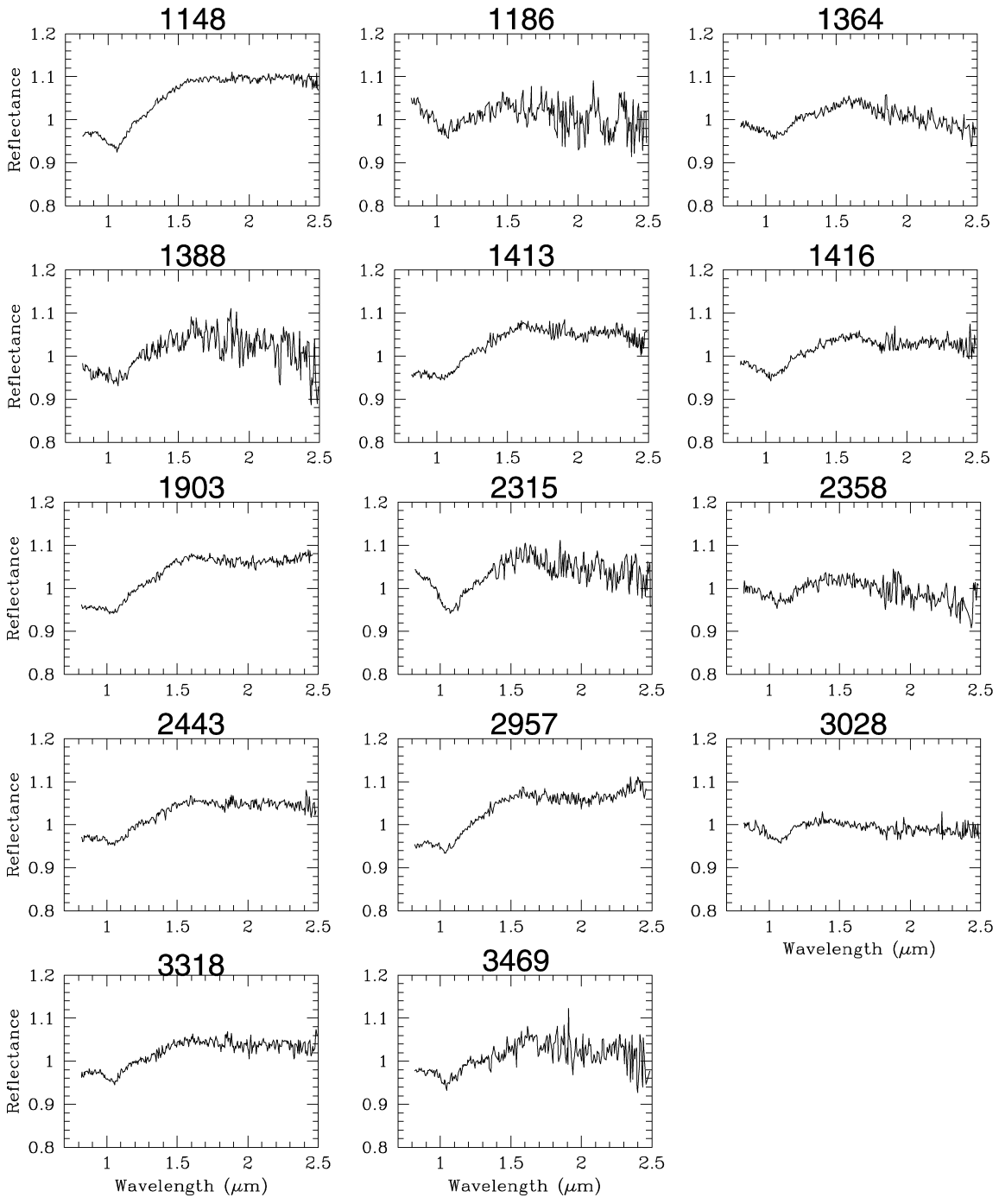

Fig. 1. (*continued*)

In methods (1) and (3) we used preferably the combined spectrum (VNIR) when it was available. The objects for which the visible was not available in public databases were analyzed only in the NIR. Some of the visible spectra were, however, too noisy, thus giving lower confidence in the results as in the case of Asteroids 590 and 798 (see Fig. 2).

4.1. Comparisons with meteorites

With the purpose of obtaining more accurate results from comparisons with meteorites, we compared all our low-resolution visible and NIR spectra of the 30 Eos family members with all meteorite spectra available from the RELAB public database (Pieters and Hiroi, 2004). For objects with spectrum in the visible range we compared the combined spectrum (VNIR). As in the work of Mothé-Diniz et al. (2005), at the moment of the comparisons, the RELAB database contained spectra of 802 meteorite samples, with more than one spectrum for some of the samples, corresponding to different grain sizes and/or observation geometry. For the comparisons we followed the method described in Mothé-Diniz et al. (2005), which consisted of a first-order automated search, creating a list of "best matches"

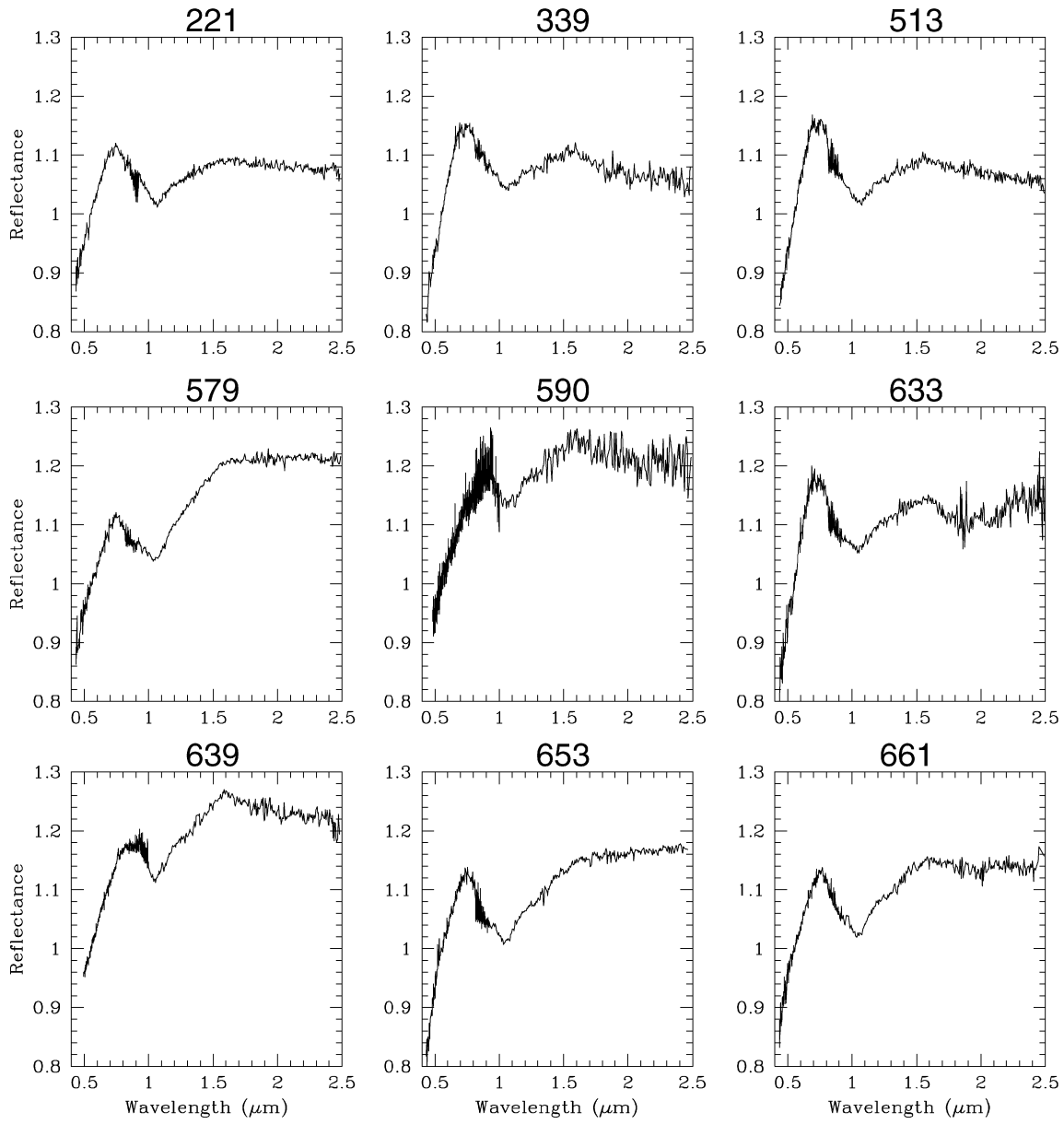

Fig. 2. Reflectance spectra for the 16 family members observed in the IRTF combined with the visible spectra. All spectra are normalized to unity at 0.55 μm.

ordered according to the dispersion between the spectrum of the asteroid and the meteorite. We then plotted the spectrum of the asteroid against the spectrum of each meteorite in the list and inspected visually those plots. In the visual inspection, we searched for similarities in the shape and position of the 1-μm absorption and of their maxima, as well as similarities in the slope along the intervals 0.5–0.8 and 1.5–2.5 μm.

In the range 0.5–1.6 μm, the anomalous achondrite Divnoe is the best analog to (221) Eos and (653) Berenike (Mothé-Diniz et al., 2005). It is also a good analog to many other objects observed in this work in the same range. However, the spectrum of this meteorite does not present the abrupt change of inclination around 1.6 μm that characterizes the spectra of most family members observed (Fig. 1). In fact, none of the meteorites presently available in the RELAB database can be considered as originally from the Eos family, from their spectral similarities. Table 2 summarizes the results of our comparisons, showing the type of the meteorites that better matches the spectra of the asteroids studied here.

CK4 and CK5 meteorites are good analogs to a large number of the family members in the NIR range only. However, in general, these meteorites have visible spectra very different from our asteroids, with a more rounded maximum around 0.7 μm. R-chondrites are also good matches to a large number of objects in our sample, in various spectral ranges, depending on the object analyzed. Globally, the R-chondrites are the meteoritic class that has the greatest number of matching features with Eos family members spectra, like the band minimum, the downturn around 1.5 μm, and the reddish steep slope in the visible (with a few exceptions among the R-chondrites). Some of the objects in our sample are also matched by CO3 and/or CV3 meteorites, mainly in the visible. Spectra of CO3 and CV3, however, have

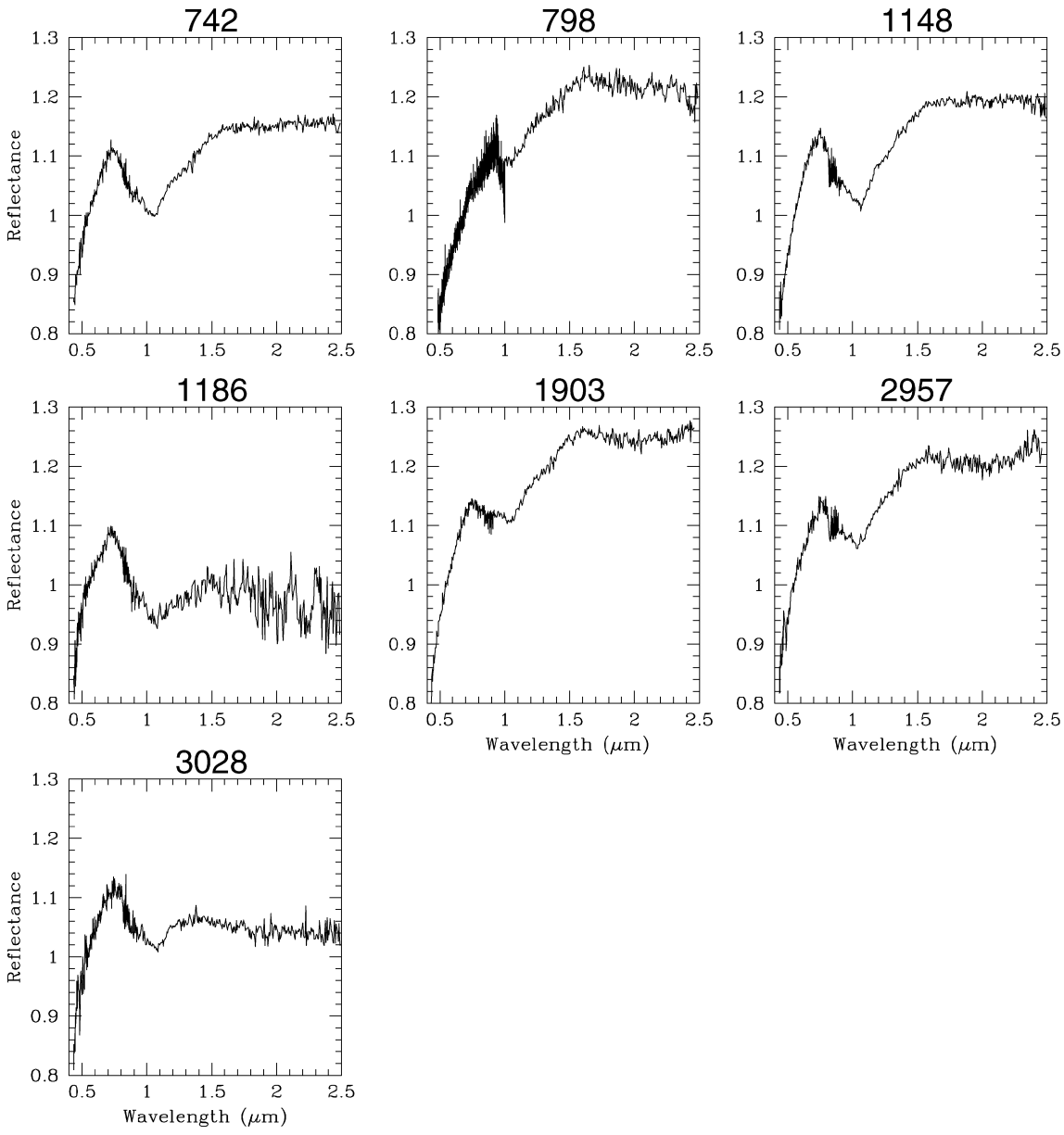

Fig. 2. (*continued*)

quite different spectra in the region around 2.0 μm, since they present a well defined pyroxene band in this region. Finally, a few objects can be matched by dunites or ureilites, usually in the region between 1.2 and 2.5 μm, and the minimum positions do not match. Additionally, in this case the dunite sample ALHA84025 is a thin section of the meteorite, while the ureilite sample measured (MP-LAM-006-C2) was the whole rock. Therefore, we conclude that this comparison is less significant than those performed on spectra of powdered samples.

Figs. 3a–3c illustrate the process described by showing the most reasonable matches to one of the asteroids in our sample, (1148) Rarahu. All matches are R-chondrites. The purpose of these plots and the discussion in this section is not to imply a direct link with any meteorite, but rather to show how difficult it can be to establish a strong mineralogical connection uniquely by comparisons with meteorites. In Fig. 3 also exhibits some of the problems that we can encounter performing this kind of comparison. In the case here presented, we have three R-chondrites, with very different spectra. Each of them is a quite good analog to the spectrum of (1148) in some wavelength range. The same happens to all other objects in the family, and with most of the asteroid spectra in general. Therefore, caution is necessary when comparing asteroid spectra with meteorites, and this kind of analysis should not be used as a sole method for inferring mineralogy of small Solar System bodies. Despite that, we can say that R-chondrites are the best meteoritic analogs to most of the objects analyzed in this paper.[3]

[3] Another problem to be considered when comparing spectra of asteroids with spectra of meteorites is the albedo. A good discussion on this topic can be found in Clark et al. (2004b) and references therein.

Table 2
Comparisons with meteorites

Number	Name	Relab sample	Type	Spectral range
221	Eos	MH-FPF-058-B	CK4	0.9–2.5 μm
339	Dorothea	LM-LAM-018	CK5	0.9–2.5 μm
450	Brigitta	MB-TXH-065-A	R	1.1–1.4 μm + 1.7–2.5 μm
$513_{[1]}$	Centesima	MH-FPF-058-B	CK4	0.9–2.5 μm
$513_{[2]}$	Centesima	MR-MJG-114-P2	CO3	0.5–1.4 μm
$579_{[1]}$	Sidonia	MB-TXH-045	R	1.1–1.4 μm
$579_{[2]}$	Sidonia	MB-TXH-045	R	0.8–1.4 μm
590	Tomyris	MH-FPF-058-A	CK4	0.9–2.5 μm
633	Zelima	MB-TXH-082	CO3	0.8–1.5 μm
639	Latona	MH-FPF-058-A	CK4	0.9–2.5 μm
653	Berenike	MB-TXH-081-A	CK4	1.1–2.5 μm
661	Cloelia	LM-LAM-008	Dunite	1.2–2.5 μm
		MB-TXH-081-A	CK4	1.1–2.5 μm
		MB-TXH-065-A	R	1.5–2.5 μm[a]
669	Kypria	RS-CMP-040	CV3	0.8–1.4 μm
742	Edisona	MB-TXH-045	R	0.8–2.5 μm
766	Moguntia	MB-TXH-065-A	R	0.8–1.4 μm[b]
798	Ruth	MS-CMP-040-B	CV3	1.1–2.3 μm
1112	Polonia	LM-LAM-008	Dunite	0.8–1.4 μm
		MP-LAM-006-C2	Ureilite	1.1–2.5 μm
1129	Neujmina	MB-TXH-065	R	1.1–1.5 μm[b]
1148	Rarahu	MB-TXH-065-A	R	0.9–2.5 μm
1186	Turnera	LM-LAM-018	CK5	0.7–2.5 μm
		MB-TXH-065	R	0.8–2.5 μm
1364	Safara	MB-TXH-077	CK4	1.0–2.5 μm
1388	Aphrodite	MB-TXH-045	R	0.8–1.5 μm
1413	Roucarie	MB-TXH-045	R	0.9–1.4 μm
1416	Renauxa	MH-FPF-055-B	CO3	0.8–2.5 μm
		MH-FPF-057-A	CV3	0.9–2.0 μm
1903	Adzhimushkaj	MS-CMP-040-B	CV3	0.8–2.5 μm
2315	Czechoslovakia	TB-TJM-114	R	1.0–2.5 μm
2358	Bahner	RS-CMP-040	CV3	0.8–1.4 μm
2443	Tomeileen	MH-FPF-055-A	CO3	0.8–1.4 μm
2957	Tatsuo	MS-CMP-040-B	CV3	1.0–2.5 μm
3028	Zhangguoxi	MR-MJG-112	CO3	0.8–1.4 μm
3318	Blixen	RS-CMP-040	CV3	1.2–2.3 μm
3469	Bulgakov	MP-LAM-006-C2	Ureilite	1.0–2.5 μm
		RS-CMP-040	CV3	1.2–2.0 μm

[a] The range indicated, plus the shape and center of 1.0 μm band.
[b] The range indicated, plus the slope in the 1.5–2.5 μm range.

The R-chondrites describe a class of meteorites named after the meteorite Rumuruti, which was the first fall of this group, discovered in the city of Rumuruti, Kenya, on 1934 January 28. Meteorites of this group can be characterized as oxidized, olivine-rich, metal-poor chondrites, that have the highest $\Delta^{17}O$ analyzed to date. They have high Fa contents in olivines of ∼39 mol%. It is well stated (Rubin and Kallemeyn, 1989, 1993; Bischoff et al., 1994) that these meteorites do not belong to carbonaceous, ordinary or enstatite chondrites, although they exhibit many characteristics typical of OCs (Weisberg et al., 1991). Unlike the other members of the class, Rumuruti itself is a fresh, unweathered meteorite. However, none of our spectra can be matched by this meteorite. Only meteorites that are "finds" have spectra that match our objects, as it is the case of samples MB-TXH-045 (ALH85151, slab), MB-TXH-065-A (PCA 91002,13, grain size <63 μm), and TB-TJM-114 (NWA753, grain size <125 μm).

4.2. MGM analysis

The modified Gaussian model (MGM) attempts to model the natural logarithm of reflectance spectra as a sum of functions of energy $x \propto 1/\lambda$, where λ is the wavelength. The continuum is modeled as a 1st degree polynomial while absorptions are represented as modified Gaussians, where the functional dependency is on x^{-1} (Sunshine et al., 1990). In the presence of noise the fits produced by the MGM tend to be non-unique, which led Sunshine and Pieters (1998) to introduce constraints during the fitting process in order to assure that the resulting band sets are mineralogically meaningful. These constraints are typically empirically-derived, loose mathematical relations among band parameters that are established through the application of the MGM to high signal-to-noise lab spectra of samples with well-characterized mineralogy. This exercise also yields calibrations that allows one to interpret the resulting MGM band parameters in terms of mineralogy (Sunshine et al., 1990;

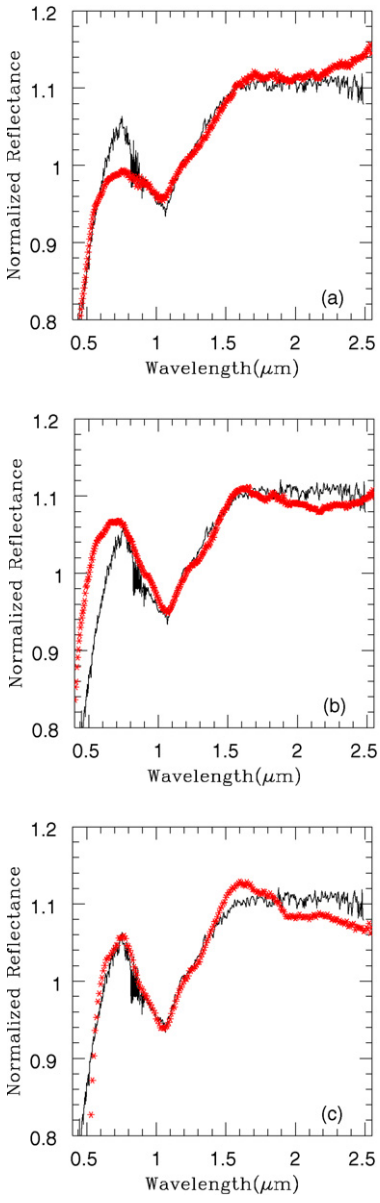

Fig. 3. Spectrum of the Asteroid (1148) Rarahu (continuous lines) compared with their best meteorite analogs (stars): (a) R-chondrite, Relab sample ALH85151; (b) R-chondrite, Relab sample PCA91002; (c) R-chondrite, Relab sample NWA753. The purpose of this plot is to show some of the problems encountered when performing comparisons with meteorites, and should not be used for further reference to infer mineralogy of the object.

Sunshine and Pieters, 1998). Presently such calibrations are restricted to olivine and pyroxene.

In the NIR, the olivine spectrum is dominated by three overlapping absorptions (with centers roughly at 0.85, 1.0 and 1.1 μm) that combine to form the characteristic broad absorption around 1 μm. These bands are formed by Fe^{2+} transitions in the M1 and M2 crystallographic sites (King and Ridley, 1987; Burns, 1993). Sunshine and Pieters (1998) showed that the centers of each band and also the ratio of the strengths of the third and first bands correlate to the forsterite content of olivine samples, and thus can be used to infer their mineralogy within an accuracy of 5%. More recently Sunshine et al. (2007) established that the band ratio calibration is temperature-dependent and therefore must be modified to match the average temperature of the asteroid. The band center calibration is, on the other hand, quite insensitive to temperature.

Table 3
Constraints used in the MGM fit

Band	Center	Width
Olivine		
1	0.825–0.925	0.21–0.28
2	1.040–1.090	0.16–0.19
3	1.200–1.300	0.40–0.51
LPC		
1	0.900–0.935	0.10–0.30
2	1.790–1.950	0.30–0.70
3	1.100–1.250	0.15–0.40
4	2.490–2.600	0.35–0.60
HCP		
1	0.910–1.060	0.10–0.30
2	1.960–2.350	0.30–0.70
3	1.200–1.300	0.40–0.51

The constraints on pyroxenes MGM fits are comparatively more relaxed. Spectra of pyroxenes contain two major absorptions around 1 and 2 μm caused by electronic transitions of Fe^{2+} in M2 sites, plus some minor absorptions. Sunshine and Pieters (1993) model orthopyroxenes (low-calcium) with the two major bands with centers loosely in the 0.9–0.95 and 1.78–1.95 μm range, plus a relatively broad and shallow band around 1.2 μm and a broad band around 2.5 μm. For clinopyroxenes (high-calcium) the authors use major bands in the 0.95–1.05 and 1.92–2.27 μm range and the 2.5 μm band is not used. Although there is presently no calibration that directly relates MGM derived parameter with pyroxene composition, one can find in the literature calibrations that links the pyroxene composition in terms of Wollastonite and Ferrosilite content with empirically derived band centers (Cloutis and Gaffey, 1991).

In order to incorporate the constraints directly into the fitting we use a custom implementation of the MGM algorithm, where the gradient-type fitting routine has been replaced by a simplex fitting algorithm (Nelder and Mead, 1965) that have been modified to perform constrained fitting (Carvano and Mothé-Diniz, in preparation). Our routine allows that constraints can be specified as absolute intervals and/or as linear relations among parameters, within a given tolerance. Here we have searched for fits using olivine and olivine/pyroxene mixtures. Table 3 shows the absolute intervals used as constraints for the pyroxene and olivine bands. Two sets of constraints were imposed on the olivine bands: (1) the position of the bands were forced to yield the same Fa composition within a 5% margin, and (2) the ratios of strengths of B_{I} and B_{II} to B_{III} are forced to stay around prescribed values. For the $B_{\mathrm{I}}/B_{\mathrm{III}}$ ratio this value is fixed at 0.6 ± 0.1, following Sunshine and Pieters (1998), while the $B_{\mathrm{II}}/B_{\mathrm{III}}$ ratio was set according to an input Fa composition, within a 5% tolerance. The relation between Fa and the $B_{\mathrm{II}}/B_{\mathrm{III}}$ ratio was obtained by interpolating Fig. 6 of Sunshine et al. (2007) to a temperature of 170 K, while the relation between Fa and band centers was taken directly from Fig. 4 of Sunshine

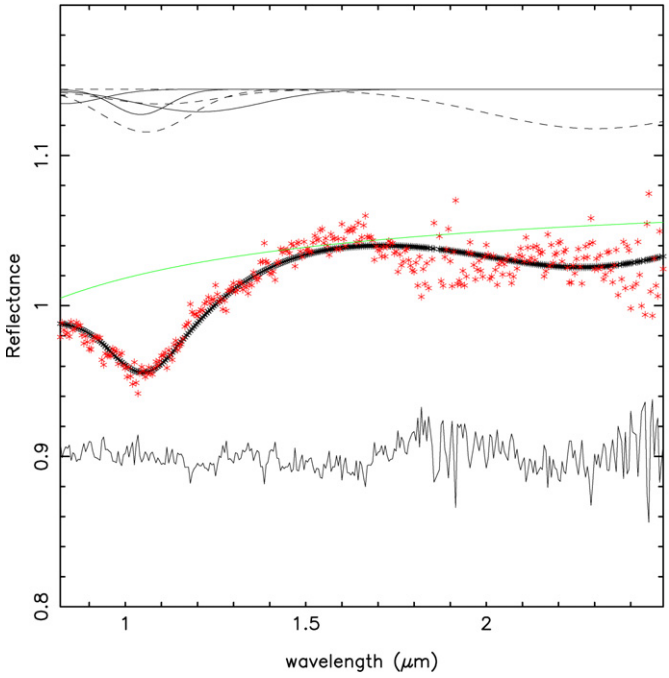

(a)

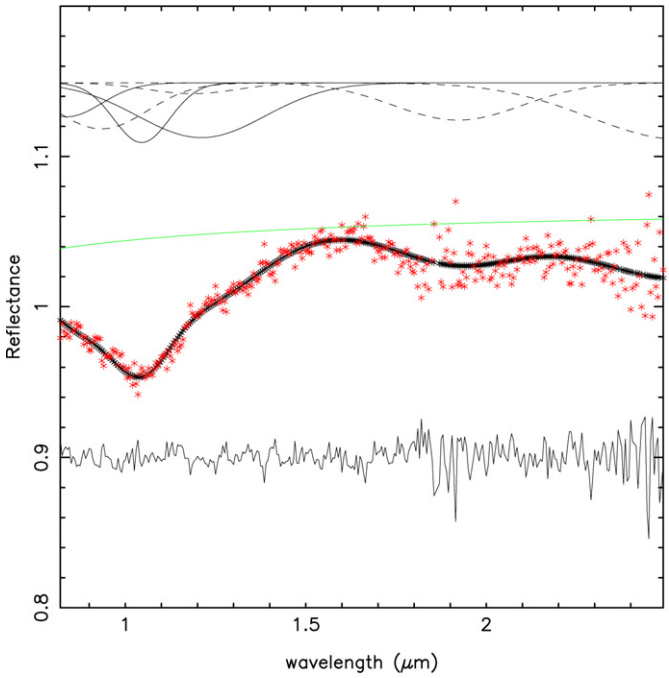

(b)

Fig. 4. Examples of MGM fits for the Asteroid (1416) Renauxa. At the top of each figure, are displayed the bands that were used in the fits (dashed lines represent pyroxene bands, and solid lines represent olivine bands). In the center of each figure the dots were used for the spectrum of the asteroid, the thick solid line for the fit, and the thin line for the continuum. At the bottom, the residuals of the fit is shown. (a) MGM fit using HCP + olivine; (b) MGM fit using LCP + olivine.

and Pieters (1998). Band widths were also constrained to be within the range observed in that paper.

Constraints for MGM band parameters of pyroxenes have not been explicitly derived in the literature. Therefore, we opted to impose restrictions during the fit so that the resulting pyroxene band parameters lie within the ranges derived in the literature from laboratory measurements. For example, the centers of the bands at 1 vs 2 μm, orthopyroxenes and clinopyroxenes tend to fall along lines with different inclinations (Adams, 1974; Cloutis and Gaffey, 1991). To ensure that the modeled pyroxenes are consistent with this trend we derived two linear relations (one for LCP and another for HCP) which express the center of the 1 μm band as function of the 2 μm band, and required that the fitted values for these two parameter follow (with a 10% margin) the trend corresponding to the type of pyroxene used.

The band strengths of 1.2 and 2 μm bands where constrained so that their ratio to the 1 μm bands stay within the values observed in Sunshine and Pieters (1993), within a 50% margin—such large margin was adopted since the pyroxenes in Sunshine and Pieters (1993) do not cover a comprehensive range in composition and because the temperature effects in pyroxene bands are presently poorly understood. The widths of the pyroxene bands were also constrained to the range of values observed in Sunshine and Pieters (1993), and all band strengths were further constrained to negative values. The systematics adopted for the fitting were as follows: the band centers and band strength ratios of the olivine bands were initialized to a given Fa composition; the resulting fit was deemed acceptable if the final Fa value derived from the band strength ratio matches within around 5% the value obtained from the band centers. For each fit, compositions ranging from Fa_0 to Fa_{100} were tried. Since not all asteroids in our sample have visible spectra, the fits were made considering only the NIR spectra, following Rivkin et al. (2004).

Using models exclusively with olivine we were able to find satisfactory fits for three asteroids only: 221, 653 and 742. For these objects the all fits found have Fa smaller than 10%. We then turned to the asteroids for which visual inspection suggested the existence of a band in the 2 μm region: 633, 669, 1413, 1416, 1903 and 2957. We initially tried models with olivine + HCP. We were able to find satisfactory fits for 633 with $Fa_{10–25}$ but with very weak olivine bands, suggesting that this asteroid could be fitted by a model with only HCP (without any olivine). For 1416 we found satisfactory fits for either Fa_{94} and Fa_8, but both show very weak olivine bands and also a poor fit in the 2 μm region. Examples of MGM fits for this object are shown in Fig. 4. For 1903 some acceptable fits were found in the range Fa_{33} to Fa_7, but these either have very weak olivine bands or presented a poor fit in the 1.2–1.5 μm range. No acceptable fits were found for 699 and 1413. Of these six asteroids with a clear 2 μm band, 2957 was the only one for which a mixture of HCP and olivine yields good fits, with olivine composition ranging from Fa_{17} to Fa_0. Using a mixture of olivine + LCP, on the other hand, all six asteroids could be successfully fit. This suggests that orthopyroxene is the dominant pyroxene species, but we cannot rule out the presence of some minor component of clinopyroxene. However, we see little point in adding more degrees of freedom to a problem that is already under-determined. Instead, we assume that all asteroids in the sample are composed of olivine + LCP mixtures, and seek for fits that are mineralogically realistic.

Using models with olivine + LCP, we were able to find satisfactory fits for all asteroids. In general, for each asteroid, more than one Fa composition yield equally good fits, and although for most asteroids the derived compositions are inside a narrow interval, some show considerable spread. The issue of interpreting the derived MGM band parameters in terms of pyroxene composition is more cloudy since for this method there are neither direct calibrations nor firm constraints for pyroxenes. Therefore we refrain from making such inferences. We find instructive, however, to try to estimate the amount of pyroxene in the assemblages. Again, there is no direct calibration to measure this quantity from MGM band parameters. Binzel et al. (2001) used the ratio of olivine to pyroxene absorption strength as a measure of the relative abundance. Here we adopt the ratio of area of the composite olivine and pyroxene bands in the 1 μm region to estimate that quantity. Explicitly, we calculate the area of the band resulting from the combination of the 1 and 1.2 μm pyroxene bands and divide it by the area of the band resulting from the combination of the three olivine bands. We assume that a higher value of this ratio indicates a greater contribution of pyroxene. The resulting fits in terms of Fa content (the average value of the band centers and band strength calibrations) and pyroxene-to-olivine area ratio for each asteroid are shown in Fig. 5. Figs. 6a and 6b show the variation of the MGM compositional values with diameter. In this figure the dots represent the central value found for a given parameter and the error bars cover the range where fits where found. Most of the asteroids in the family have fits consistent with a composition of $\sim Fa_{20}$ (Fo_{80}, forsterite content). Only seven asteroids do not shown any fit in this range, and those tend to have fits that overlap around a composition of $\sim Fa_{40}$. A few asteroids have fits with fayalite contents as low as Fa_4. Three asteroids also have very high Fa values but those are also the ones with the higher spread in the Fa content and typically are the ones with noisier spectra. Concerning the pyroxene content, most of the asteroids have fits that overlap around a pyroxene-to-olivine area ratio of ∼0.1. Four asteroids do not show any fit consistent with this value and tend to overlap around 0.2; four asteroids that also do not have any fit around 0.1 tend to overlap around 0.05. Among the asteroids with values higher than 0.1 of the pyroxene-to-olivine area ratio is 633, which show values of this parameter as high as 0.62, albeit with considerable scatter. The Asteroid (221) Eos, on the other hand, shows the lowest pyroxene-to-olivine area values, with no fit with a value greater than 0.04 found. Although no clear trend with diameter is seen in Fig. 6, it is noteworthy that the biggest fragment, (221) Eos, has also forsterite contents that are among the highest. Indeed, the three biggest fragments are compatible with a trend of increasing forsterite and decreasing pyroxene contents with increasing diameter, although the significance of a correlation with only three points cannot be properly assessed.

4.3. Hapke analysis

In order to constrain the composition of the spectra of the Eos family members, we also used a mixing model that simulates the conditions of intimately mixed particles of some given minerals at the surface of an asteroid. Then, we minimize the difference between the model mixture and the asteroid spectrum. To model the reflectance spectra of mixtures of material we used the expression for the bidirectional reflectance from Hapke (1993):

$$r_\lambda(\mu, \mu_0, g) = \frac{w_\lambda}{4\pi}\frac{\mu}{\mu+\mu_0}\big[p(g) + H(\mu_0)H(\mu) - 1\big], \tag{1}$$

where w_λ is the wavelength-dependent single scatter albedo, μ, μ_0 and g are, respectively, the cosine of the emission angle, the cosine of the incidence angle and the phase angle, $p(g)$ is the phase function and $H(X)$ is the Chadrasekhar H function that can be approximated by

$$H(X) = \frac{1+2X}{1+2X\sqrt{1-w_\lambda}}. \tag{2}$$

For the phase function we used a Legendre expansion with the form:

$$p(g) = 1 + b\cos(g) + c\big(1.5\cos^2(g) - 0.5\big), \tag{3}$$

where the coefficients b and c for silicates are, respectively, 0.2 and −0.4, and 0.2 and 0.3 for opaques (Mustard and Pieters, 1989).

The expression for the reflectance is an approximate solution of the radiative transport equation where it is assumed that the medium is composed by isotropic scatters that are large compared with the wavelength. For intimate mixtures of M end-members, the effective single scatter albedo of the particles is given by Mustard and Pieters (1989) and Hapke (1993):

$$w_\lambda = \frac{\sum_j^M N_j\sigma_j w_{\lambda j}}{\sum_j^M N_j\sigma_j}, \tag{4}$$

where for each particle type σ is the effective cross-section and N is the numeric density.

The single scatter albedo of the end-members was obtained from reflectance measurements taken in the lab, by numerically inverting Eq. (1), using the same phase function assumed for the asteroid spectra. This approach is similar to the one of Clark et al. (2004a). Alternatively, the single scatter albedo could have been calculated from optical constants assuming a geometrical optics approximation (Hapke, 1993). We opted not to do this because the optical constants that are publicly available for olivine and pyroxenes span a range of compositions that are much more limited than what is available from reflectance spectra. A downside to the adopted approach is that we lose the ability to vary the grain size during the fit, since the grain size is fixed by the size distribution of the laboratory samples. We however do not think that this is actually a problem, since most measured samples have grain sizes in the ranges that are believed to occur on asteroidal regoliths, and often several samples with different particle sizes are available for a given material.

The spectra of minerals used in the mixtures were taken from two public databases: RELAB (Pieters and Hiroi, 2004) and USGS Digital Spectral Library (USGS, 2006), and its main characteristics are shown in Table 4. To select the olivine phase we have tried all the spectra available in RELAB and USGS databases, with compositions ranging from Fa_8 to Fa_{89}.

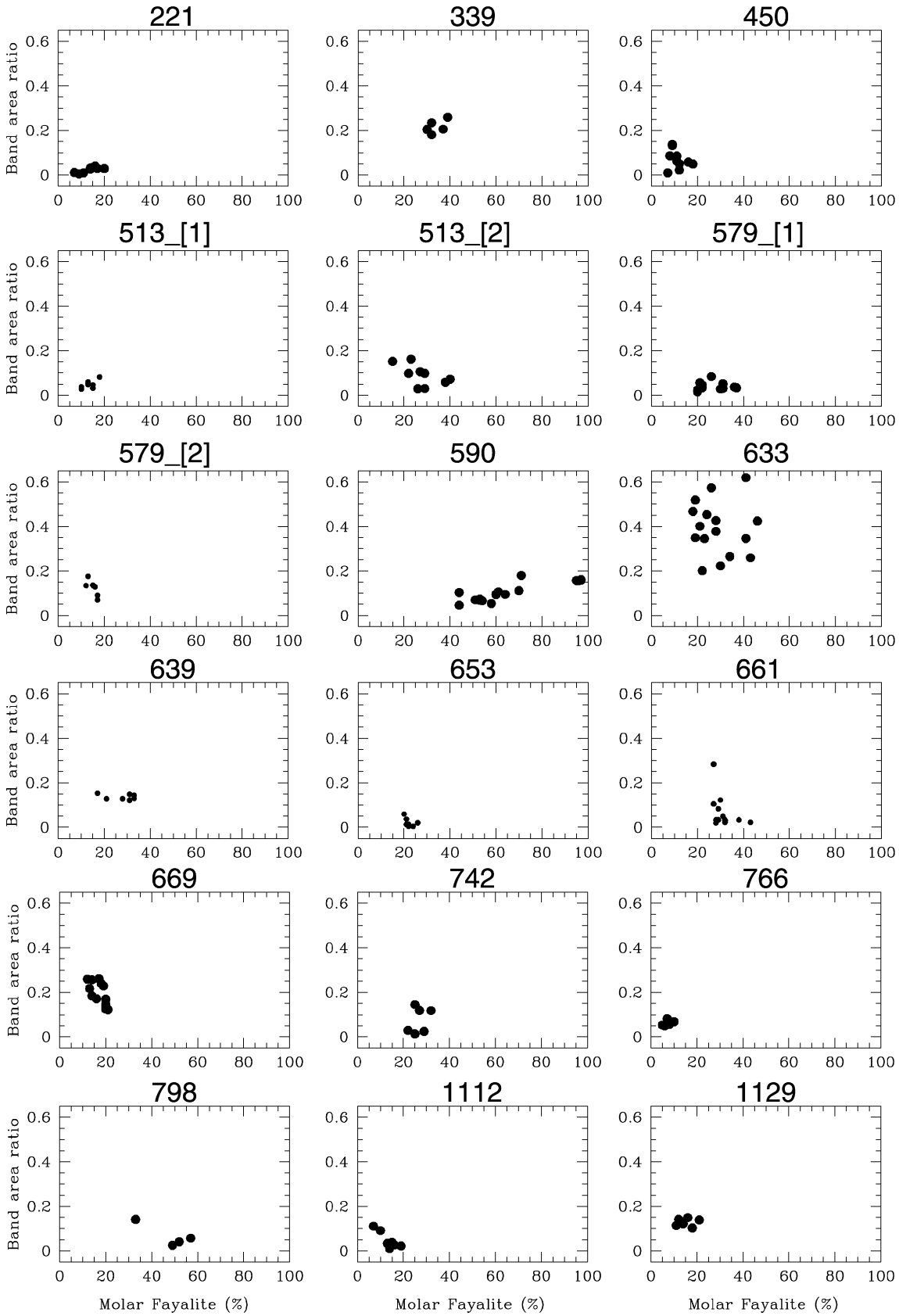

Fig. 5. Plots showing, for each object in the Eos family, the percentage of the molar forsterite derived from the MGM analysis against the pyroxene to olivine band area ratio.

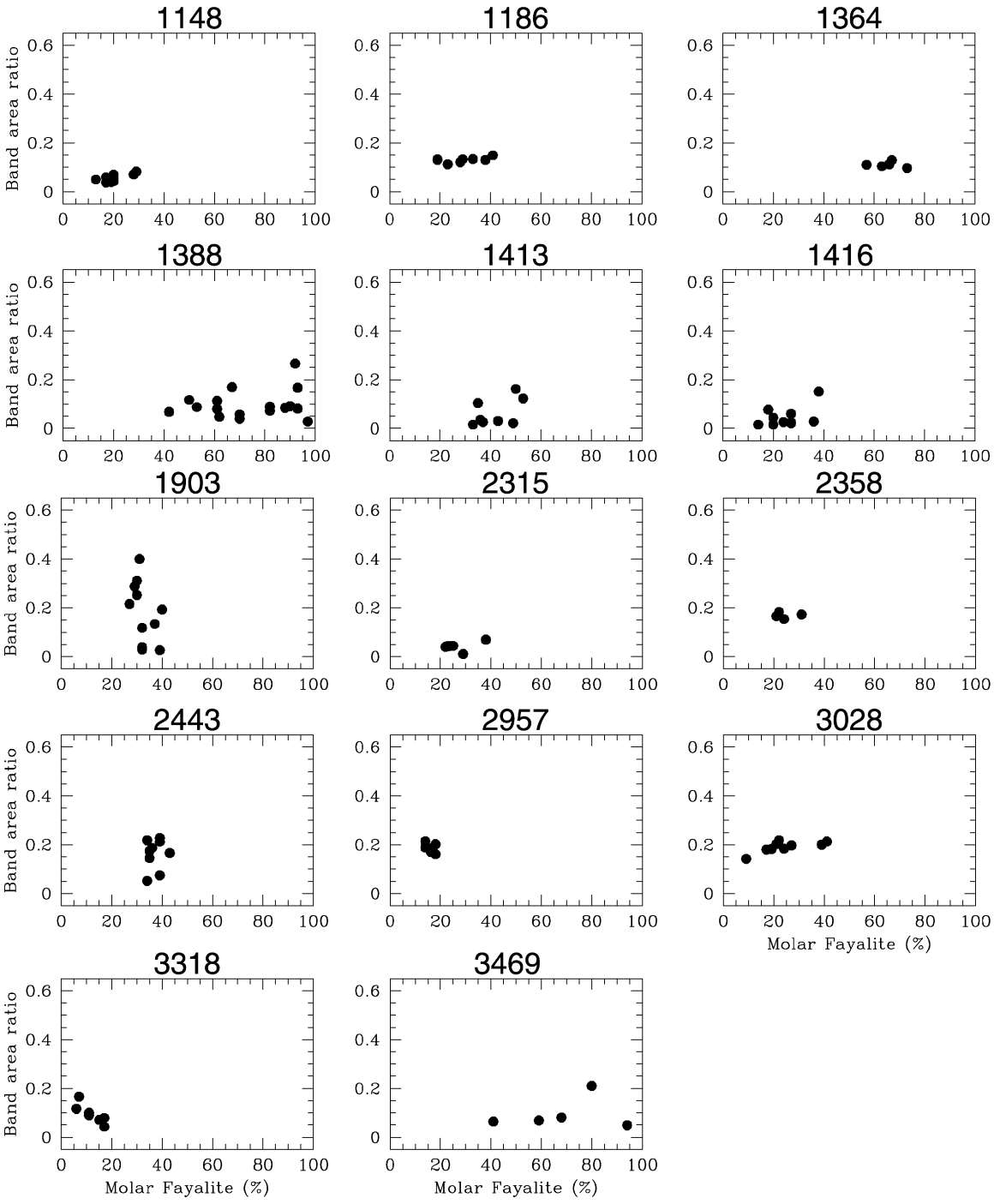

Fig. 5. (*continued*)

Only three olivine spectra produced acceptable fits: the gds71b (olivine Fa_8 from USGS), cxms05 (olivine $Fa_{13.5}$ from the Meteorite Pallasite Marjalahti) and c1rb43 (olivine tholecite, sample of primitive aluminum rich basalt, for which the Fa content was not available in RELAB). Different pyroxenes and low-phase minerals were also tested until we had a good fit. In our case, the low-phase mineral that provided the best fits was the volcanic ash glass (sample c1rb50), which served mainly to reduce the contrast of the absorptions. Other minerals such as carbon can also provide acceptable fits for some of the spectra. The iron oxide was added since until the addition of this mineral we were not able to fit the strong slope of the spectra in the visible range. The addition of iron oxide and glass simulates to some extent the effects of space-weathering, since the former end-member promotes a reddening of the spectra, while the latter reduces the contrast of the bands.

The spectra of the end-members used in the mixing model are shown in Figs. 7 and 8. Table 5 provides model abundances for each object.

As a test for our analysis method and relevance of the results of this section, we also used the Hapke method to examine laboratory spectrum of the meteorite Divnoe (sample MB-CMP-

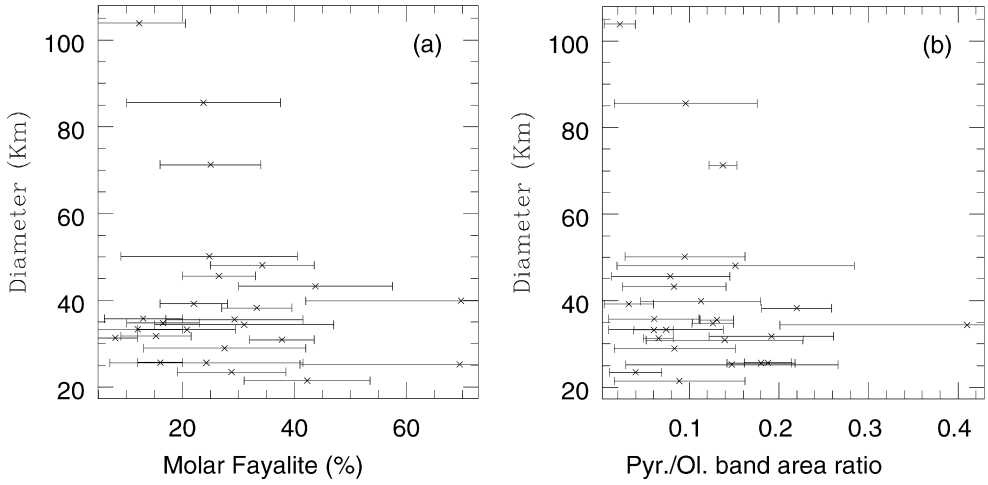

Fig. 6. Plots showing the variation with the diameter of: (a) amount of molar forsterite and (b) amount of pyroxene in the mixture. This last quantity, as stated in the text, is proportional to the true abundance, and not a calibrated value.

Table 4
Mineral end-members used in Hapke mixture model described in the text

File name	Name	Mix code	Grain size (μm)	Comments
gds71b (USGS)	Olivine	Oli1	< 60	Fa8
cxms05 (RELAB)	Meteorite pallasite	Oli9	<40	Fa13.5
c1rb43 (RELAB)	Olivine tholecite	Oli10	<30	–
c1po44 (RELAB)	Olivine	Oli12	<30	Fa21
capp47 (RELAB)	Orthopyroxene bronzite	Opx3	<45	–
c1rb50 (RELAB)	Basaltic glass ash	Glass1	<1000	–
c1io02 (RELAB)	Iron oxide	IronOx1	<3	–

Notes. The first column contains the name of every sample and database from where its spectrum was taken. The third column lists the labels that we used for every mineral during the mixing process. The fourth column lists the grain-size of every sample, and the last column lists its mineral composition in terms of the fayalite content Fa, whenever it was available in the database.

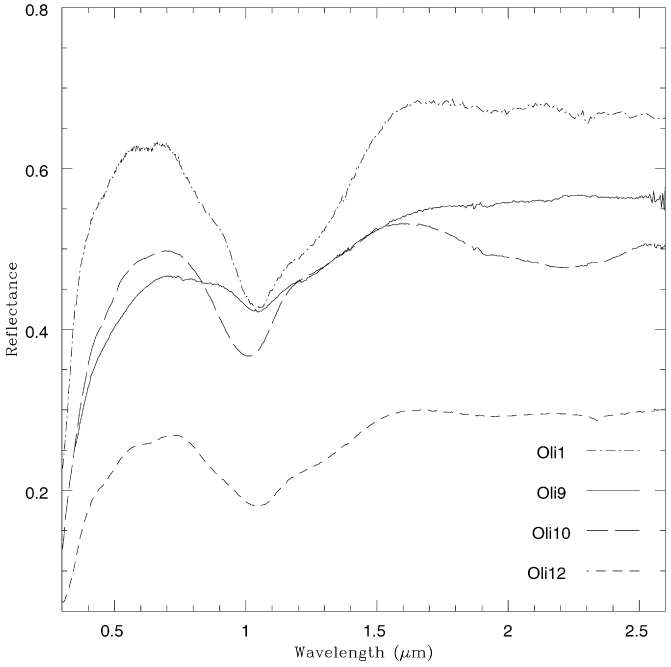

Fig. 7. Spectra of olivines used as end-members in the mixing model. Oli1 is the sample gds71b from the USGS database. Oli9, Oli10 and Oli12 stand for samples mxms05, c1rb43 and c1po44 from RELAB. More details on the characteristics of these samples are given in Table 4.

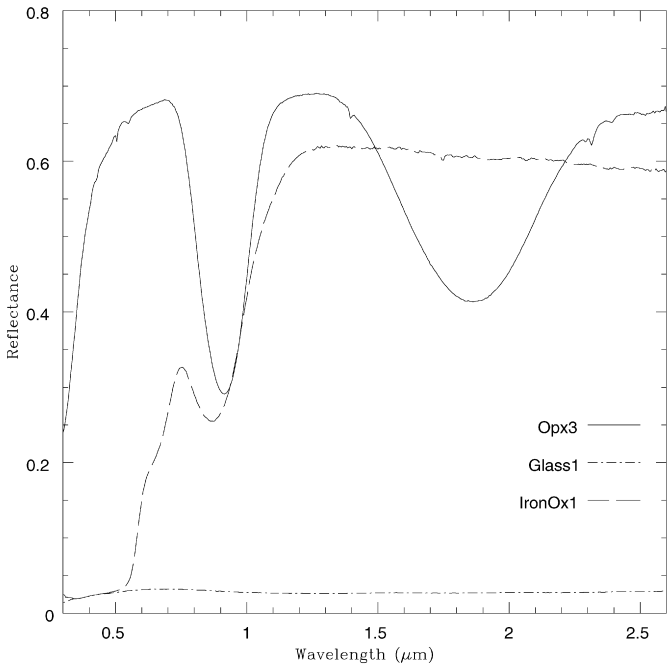

Fig. 8. Spectra of the orthopyroxene, glass and iron oxide used as end-members in the mixing model.

Table 5
Mixing model results

Asteroid	Name	Oli1	Oli9	Oli10	Opx3	Glass1	IronOx1
221	Eos	98	0	0	<1	<1	<1
339	Dorothea	0	0	95	0	3	2
450	Brigitta	98	0	0	0	<1	2
$513_{[1]}$	Centesima	0	0	94	0	3	3
$513_{[2]}$	Centesima	99	0	0	0	<1	1
$579_{[1]}$	Sidonia	0	100	0	0	Traces	<1
$579_{[2]}$	Sidonia	0	98	0	0	0.09	1.1
590	Tomyris	98	0	0	0	<1	<1
633	Zelima	88	0	0	11	<1	<1
639	Latona	98	0	0	0	<1	1
653	Berenike	97	0	0	2	<1	<1
661	Cloelia	97	0	0	2	<1	<1
669	Kypria	92	0	0	6	<1	1
742	Edisona	96	0	0	3	<1	<1
766	Moguntia	99	0	0	0	<1	<1
798	Ruth	98	0	0	0	<1	2
1112	Polonia	98	0	0	0	<1	<1
1129	Neujmina	99	0	0	0	<1	0
1148	Rarahu	97	0	0	2	Traces	<1
1186	Turnera	0	0	94	3	3	<1
1364	Safara	0	0	97	0	1	2
1388	Aphrodite	97	0	0	0	<1	2
1413	Roucarie	97	0	0	0	<1	2
1416	Renauxa	0	0	98	0	<1	2
1903	Adzhimushkaj	95	0	0	3	1	<1
2315	Czechoslovakia	100	0	0	0	<1	Traces
2358	Bahner	0	0	97	0	2	1
2443	Tomeileen	98	0	0	0	<1	2
2957	Tatsuo	0	95	0	4	<1	<1
3028	Zhangguoxi	0	0	96	0	2	2
3318	Blixen	98	0	0	0	<1	2
3469	Bulgakov	98	0	0	0	<1	1

015-D). We were not able to fit the spectrum of Divnoe with any of the three olivines used to fit the spectra of the family members. However, the olivine sample PO-RGB-044, Oli12 in Table 4, with composition Fa21 gives an excellent fit, together with some iron oxide and glass. This olivine is in agreement with the olivine composition of the meteorite: $Fa_{20–28}$. Since we were able to determine the mineralogy of a meteorite with known composition, we believe we can be confident on our results for asteroids of unknown composition.

As we can see in Table 5, the largest remnant of the breakup of the family, (221) Eos, as well as most of the objects are best fitted with the olivine gds71b from USGS, with composition Fa_8 (Oli1), plus minor amounts or traces of volcanic ash glass and iron oxide. Small amounts of orthopyroxene bronzite (<11%) is also present in some of them. Two of the Eos family members (579 and 2957) were best fitted with olivine from the Meteorite Pallasite Marjalahti from RELAB (sample cxms05, here called Oli9) with composition $Fa_{13.5}$ instead of the olivine gds71b. Other five objects (339, 513, 1186, 1416 and 3028) needed a different olivine to produce acceptable fits. For them, the sample used was the c1rb43 of olivine tholecite from RELAB (Oli10). Small amounts of orthopyroxene bronzite were needed to fit nine objects: 221, 633, 653, 661, 669, 742, 1148, 1186 and 2957. Fig. 9 illustrates the results of the mixing model, by showing the best fit for Asteroid (661) Cloelia. As

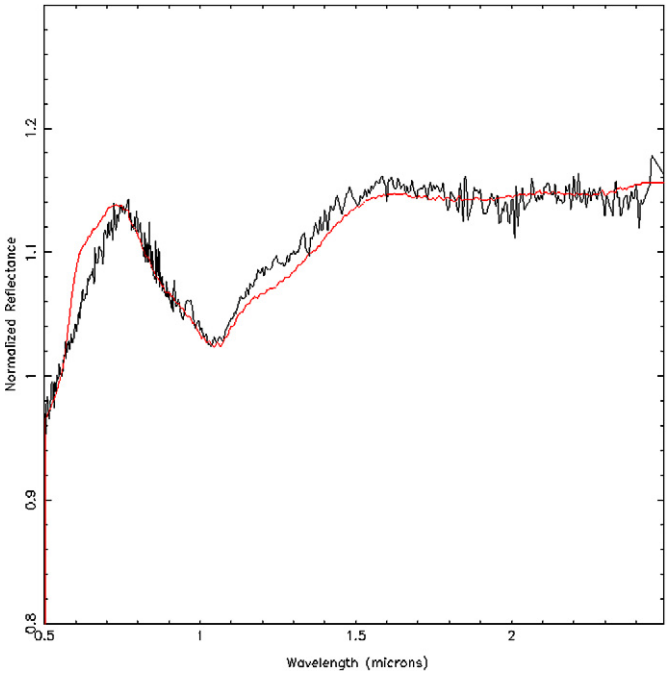

Fig. 9. Mixing model result for the Asteroid (661) Cloelia, using composition given in Table 5.

for all objects fitted, we can reproduce very well the shape and position of the center of the 1.0 μm band, and the overall shape of the spectrum from 0.8 μm on. In some cases, as shown in the figure for (661) Cloelia, we see a small difference in the visible part of the spectrum, around 0.6 μm, which we were not able to minimize with other materials.

5. Discussion

The compositional modeling methods used in this paper suggest that most of the Eos family members are compatible with surface compositions dominated by forsteritic olivine with Fa content around 20% or smaller and a minor contribution of LCP. In particular, the Asteroid 766, whose spectra has only a modest amount of noise, only have fits that are tightly clustered around Fa_{10}. Direct comparisons with meteorites in general fail to find good matches, the best candidates being the CK-chondrites and with R or even CO/CV meteorites as other possible candidates. A moderately forsteritic composition ($Fa_{40–60}$), as it is suggested from the MGM analysis for some family members, would be consistent with a carbonaceous chondrite or an R chondrite composition.

A key question here is which are the processes capable of producing bodies with compositions dominated by highly magnesian olivine. According to Sunshine et al. (2007), compositional analysis of meteorite samples suggest that for the chondrites the amount of olivine is anticorrelated with the forsterite content in the olivine. Thus, Sunshine et al. (2007) suggest that nebular oxidation processes might be incapable of producing olivine-rich chondrite with highly forsteritic composition. On the other hand, simulations show that partial melting of a chondrite produces early silicate partial meltings enriched in plagioclase and pyroxene and more ferroan than the residue: olivines

$Fa_{10–12}$ + minor LCP can be produced as residues of 45–70% partial melting at $T \sim 1400$–$1500\,^{\circ}C$ of an H-chondrite (Sunshine et al., 2007).

Following this line of arguments, our results would suggest that the Eos family might be composed by pieces of the mantle of a parent-body formed by the partial melting of ordinary chondrite material. This view is consistent with the trend of both pyroxene and forsterite contents with diameter, that we see for the three largest fragments (see Section 4.2). It is particularly interesting that the largest fragment (221) Eos has both very low pyroxene and very high forsterite contents. We must stress however that the rationale of Sunshine et al. (2007) is based on empirical evidence. It is not clear from nebular condensation models whether or not it is possible to form a highly forsteritic olivine body without differentiation.

To address this possibility, that the Eos family might be differentiated, we must take into account also the large spread in (1) the spectral slope at visible wavelengths (responsible for the taxonomic diversity) and (2) the geometric albedo of the family members (see Table 1).

Concerning the first point, Doressoundiram et al. (1998) originally ascribed the slope variation to space weathering effects. Space weathering is the general name given to a myriad of processes that modify the optical properties of materials on the surface of airless bodies, which include impacts, solar wind implantation, sputtering by energetic particles and micrometeorite bombardment (Clark et al., 2002 and references therein). The current prevailing view is that vapor deposition of submicroscopic iron particles, caused by ion sputtering and micrometeorite impacts, would be the dominant space weathering process for asteroids. The coating by the submicroscopic iron particles produces spectral reddening, reduces band depth and decreases the albedo of clear silicates, with the spectral changes being more intense in the visible part of the spectrum than at longer wavelengths. This last point in particular is in qualitative agreement with a taxonomic diverse family in the visible being relatively homogeneous in the NIR.

Regarding the albedo, space weathering is also a possible explanation for the spread in the geometric albedo in the family. It is important to notice that the geometric albedo depends on the shape of the body as well as on the scattering properties of the surface material.

Given that at this point we have two possible scenarios for the family (differentiated, dunite-like compositions or primitive chondritic parent-body), we found instructive to compare the geometric albedo that would be observed for bodies with olivine-dominated mantle material (dunite) and that of chondritic material. Single scattering albedo measurements of laboratory sample are still scarce in the literature, but Kamei and Nakamura (2002) derived single scatter albedos and phase-function parameters for samples of forsteritic dunite and the CV3 meteorite Allende. Assuming a spherical shape and using the single scatter and asymmetry parameters of Kamei and Nakamura (2002), we estimated that the observed visible geometric albedo for CV-like material would be $p_v = 0.25$, while for dunites we would have $p_v = 0.43$; non-spherical convex shapes would yield somewhat higher geometric albedos. Direct comparison of these values with the geometric albedos of the Eos family members would suggest a CV-like composition for the family. This rationale however does not consider space weathering processes. The effects of space weathering on olivine samples have recently been subject of several studies (Brunetto et al., 2006; Brunetto and Strazzulla, 2005; Marchi et al., 2005; Hiroi and Sasaki, 2001) and include extreme increase in the spectral slope and reduction in the reflectance that can be up to a factor of 2.5 in 0.55 μm (from Fig. 2 of Brunetto et al., 2006). Since to first approximation reflectance is proportional to single scatter albedo this suggests a similar reduction in this parameter. Thus, even the lower end of the geometric albedo distribution observed in the family members could be explained by space weathering acting on a dunite-like composition. Indeed, the other asteroids for which an olivine-dominated Mg-rich compositions were inferred show a wide range of geometric visible albedos (Table 6).

Table 6
Table showing the wide range of geometric visible albedos for olivine-dominated Mg-rich asteroids, reported by previous authors

Asteroid	Name	p_v	Reference
246	Asporina	0.1744	Sunshine et al. (2007)
289	Nenetta	0.2438	”
354	Eleonora	0.1948	”
446	Aeternitas	0.2361	”
863	Benkoela	0.5952	”
984	Greta	0.423	”
1951	Lick	0.0895	de León et al. (2004)

On carbonaceous chondrites effects of space weathering are less well understood. Evidences from the study of CI/CM chondrites suggest that at least solar wind sputtering does not alter significatively the optical properties of these materials. On the other hand, Sasaki et al. (2004) reported laboratory space weathering simulations on samples of the CV3 meteorite Allende that suggest some degree of alteration taking place.

If we assume that CV-like materials are not affected by space weathering processes, then it makes sense that the higher geometric visible albedo found among family members are directly comparable with the geometric albedo of a body covered with CV material, and all albedo variations could be due to differences in shape and/or minor compositional variations amongst the family members. We however would have to invoke some other mechanism to explain the variations in the spectral slope; one possible would be the mineralogical variation induced by thermal metamorphism in the parent body. Conversely, if we assume that CV material is affected by space weathering then the spread in the albedo and spectral slope seen in the family can be explained. But then we would have to assume that at least the four members of the family which have $p_v > 0.25$ suffered recently a major resurfacing event, which does not seem reasonable. Note however that the preceding discussion assumes that space weathering effects on CV materials, if any, would be similar to what is observed on olivines and pyroxenes, and even that is presently uncertain.

Finally, it would be instructive to compare the band depths of the spectra of Eos family members with other asteroids that

have been inferred to have olivine-rich compositions, such as those listed in Table 6. A remarkable difference is that the Eos family spectra in general show a much weaker 1.0 μm band. The reason of this difference is not clear. Space weathering acting on similar compositions cannot be claimed as an explanation for the difference, since both sets of asteroids present similar albedo ranges. It is worth to note here that, for both sets, the possibly differentiated composition was inferred based on the olivine compositions derived. It is not obvious whether a differentiation assemblage should present a deep or shallow band only. Indeed, a look at the RELAB database shows that dunite-like material can be found with both weak and deep bands, depending on the accessory phases present. At any rate, what can be said for sure is that, despite the similar olivine composition, Eos family members must have an overall different mineralogy than the other magnesian–olivine asteroids studied so far.

6. Conclusion

In the end, a final answer to whether or not the Eos family formed from a differentiated parent body still seems elusive. The overall composition of the family and the presence of a member whose spectra is dominated by olivine with $Fa_{04–12}$ would suggest, in the light of the rationale put forward by Sunshine et al. (2007), that the family is differentiated. In this case the range of compositions found would be due to the compositional gradient inside the parent body and the spread and values of the albedos in the family could be understood as effects of space weathering acting on dunite-like material. If we assume that the Eos family is differentiated, then its parent-body cannot have been formed in the present position of the family. The background of the family is dominated by C-type asteroids with an implied carbonaceous chondrite composition. The partial differentiation of a carbonaceous chondrite body is not supposed to produce the high contents of forsterite in the olivine that is implied for the family. As mentioned above, such a composition could be produced by partial differentiation of ordinary chondrite material. Meteoritic evidences suggest that the ordinary chondrites formed closer to the Sun than the carbonaceous chondrites. Then, the parent-body of the family must have formed at smaller heliocentric distances than the present location of the family.

On the other hand, many family members have compositions that are compatible with chondrites, and it is not completely clear that nebular processes are incapable of producing bodies dominated by highly forsteritic olivine. CK chondrite-like compositions are a viable option, since they have compatible olivine compositions and similarities in the spectra. Also, carbonaceous chondrites in general seem to be more common in the outer main-belt. This seems to be a simpler explanation, since the differentiation scenario would require the migration of the parent-body of the family from the inner to the outer main belt. If the composition is CK-like, then the variation of the composition and albedo in the family could be ascribed to metamorphism in the parent body, but the distribution of the albedos would be difficult to explain if the effects of space weathering on chondrites is important. A possible way to settle the question could then come from a better understanding of space weathering effects on CK, R and CV chondrites. If a significant decrease in albedo is detected as a result of the exposure of these materials then a differentiated parent body for the Eos family would be favored.

Acknowledgments

We thank Dr. Jessica Sunshine for the long discussions that much improved this manuscript and also to the anonymous reviewer for the very helpful comments and suggestions. This work has been supported by the *Conselho Nacional de Desenvolvimento Científico e Tecnológico*–CNPq/Brazil. This research utilizes spectra acquired with the NASA RELAB facility at Brown University.

References

Adams, J.B., 1974. Visible and near-infrared diffuse reflectance spectra of pyroxenes as applied to remote sensing of solid objects in the Solar System. J. Geophys. Res. 79, 4829–4836.

Bell, J.F., 1988. A probable asteroidal parent body for the CV or CO chondrites. Meteoritics 23, 256–257.

Binzel, R.P., Rivkin, A.S., Bus, S.J., Sunshine, J.M., Burbine, T.H., 2001. MUSES-C target Asteroid 1998 SF36: A reddened ordinary chondrite. Meteorit. Planet. Sci. (Suppl.) 36, 20.

Bischoff, A., Geiger, T., Palme, H., Spettel, B., Schultz, L., Scherer, P., Loeken, T., Bland, P., Clayton, R.N., Mayeda, T.K., Herpers, U., Meltzow, B., Michel, R., Dittrich-Hannen, B., 1994. ACFER 217—A new member of the Rumuruti chondrite group (R). Meteoritics 29, 264–274.

Brunetto, R., Strazzulla, G., 2005. Elastic collisions in ion irradiation experiments: A mechanism for space weathering of silicates. Icarus 179, 265–273.

Brunetto, R., Romano, F., Blanco, A., Fonti, S., Martino, M., Orofino, V., Verrienti, C., 2006. Space weathering of silicates simulated by nanosecond pulse UV excimer laser. Icarus 180, 546–554.

Burbine, T.H., Binzel, R.P., Bus, S.J., Clark, B.E., 2001. K asteroids and CO3/CV3 chondrites. Meteorit. Planet. Sci. 36, 245–253.

Burns, R.G., 1993. Mineralogical Applications of Crystal Field Theory. Cambridge Topics in Mineral Physics and Chemistry. Cambridge University Press, New York.

Bus, S.J., Binzel, R.P., 2002. Phase II of the small main-belt asteroid spectroscopic survey: The observations. Icarus 158, 106–145.

Clark, B.E., Hapke, B., Pieters, C., Britt, D., 2002. Asteroid space weathering and regolith evolution. Asteroids III, 585–599.

Clark, B.E., Bus, S.J., Rivkin, A., McConnochie, T., Sanders, J., Shah, S., Hiroi, T., Shepard, M., 2004a. E-type asteroid spectroscopy and compositional modelling. J. Geophys. Res. 109, 2001.

Clark, B.E., Bus, S.J., Rivkin, A., McConnochie, T., Sanders, J., Shah, S., Hiroi, T., Shepard, M., 2004b. Spectroscopy of X-type asteroids. Astron. J. 128, 3070–3081.

Cloutis, E.A., Gaffey, M.J., 1991. Pyroxene spectroscopy revisited: Spectral-compositional correlations and relationships to geothermometry. J. Geophys. Res. 96, 22,809–22,826.

de León, J., Duffard, R., Licandro, J., Lazzaro, D., 2004. Mineralogical characterization of A-type Asteroid (1951) Lick. Astron. Astrophys. 422, L59–L62.

Doressoundiram, A., Barucci, M.A., Fulchignoni, M., Florczak, M., 1998. Eos family: A spectroscopic study. Icarus 131, 15–31.

Gaffey, M.J., 1976. Spectral reflectance characteristics of the meteorite classes. J. Geophys. Res. 81 (10), 905–920.

Hapke, B.W., 1993. Theory of Reflectance and Emittance Spectroscopy. Cambridge University Press, New York.

Hiroi, T., Sasaki, S., 2001. Importance of space weathering simulation products in compositional modeling of Asteroids: 349 Dembowska and 446 Aeternitas as examples. Meteorit. Planet. Sci. 36, 1587–1596.

Kamei, A., Nakamura, A.M., 2002. Laboratory study of the bidirectional reflectance of powdered surfaces: On the asymmetry parameter of asteroid photometric data. Icarus 156, 551–561.

King, T.V.V., Ridley, W.I., 1987. Relation of the spectroscopic reflectance of olivine to mineral chemistry and some remote sensing implications. J. Geophys. Res. 92, 11,457–11,469.

Lazzaro, D., Angeli, C.A., Carvano, J.M., Mothé-Diniz, T., Duffard, R., Florczak, M., 2004. S^3OS^2: The visible spectroscopic survey of 820 asteroids. Icarus 172, 179–220.

Lord, S., 1992. A new software tool for computing Earth's atmospheric transmission of near- and far-infrared radiation. NASA Tech. Memo., TM103957, 194.

Marchi, S., Brunetto, R., Magrin, S., Lazzarin, M., Gandolfi, D., 2005. Space weathering of near-Earth and main belt silicate-rich asteroids: Observations and ion irradiation experiments. Astron. Astrophys. 443, 769–775.

Mothé-Diniz, T., Carvano, J.M., 2005. 221 Eos: A remnant of a partially differentiated parent body? Astron. Astrophys. 174, 54–80.

Mothé-Diniz, T., Roig, F., Carvano, J.M., 2005. Reanalysis of asteroid families structure through visible spectroscopy. Icarus 174, 54–80.

Mustard, J.F., Pieters, C.M., 1989. Photometric phase functions of common geologic minerals and applications to quantitative analysis of mineral mixture reflectance spectra. J. Geophys. Res. 94, 13,619–13,634.

Nelder, J.A., Mead, R., 1965. A simplex method for function minimization. Comput. J. 7, 308–313.

Pieters, C.M., Hiroi, T., 2004. RELAB (Reflectance Experiment Laboratory): A NASA multiuser spectroscopy facility. Lunar Planet. Sci. Abstract 1720.

Rivkin, A.S., Binzel, R.P., Sunshine, J., Bus, S.J., Burbine, T.H., Saxena, A., 2004. Infrared spectroscopic observations of 69230 Hermes (1937 UB): Possible unweathered endmember among ordinary chondrite analogs. Icarus 172, 408–414.

Rubin, A.E., Kallemeyn, G.W., 1989. Carlisle Lakes and Allan Hills 85151—Members of a new chondrite grouplet. Geochim. Cosmochim. Acta 53, 3035–3044.

Rubin, A.E., Kallemeyn, G.W., 1993. Carlisle Lakes chondrites: Relationship to other chondrite groups. Meteoritics 28, 424.

Sasaki, S., Ueda, Y., Loeffler, M., Hiroi, T., 2004. Laboratory simulation of changes of asteroid reflectance spectra by space weathering: Pulse laser irradiation on meteorite samples. In: 35th COSPAR Scientific Assembly. COSPAR Plenary Meetings, vol. 35, p. 3732.

Sunshine, J.M., Pieters, C.M., 1993. Estimating modal abundances from the spectra of natural and laboratory pyroxene mixtures using the modified Gaussian model. J. Geophys. Res. 98 (17), 9075–9087.

Sunshine, J.M., Pieters, C.M., 1998. Determining the composition of olivine from reflectance spectroscopy. J. Geophys. Res. 103 (12), 13,675–13,688.

Sunshine, J.M., Pieters, C.M., Pratt, S.F., 1990. Deconvolution of mineral absorption bands—An improved approach. J. Geophys. Res. 95 (14), 6955–6966.

Sunshine, J.M., Bus, S.J., McCoy, T.J., Burbine, T.H., Corrigan, C.M., Binzel, R.P., 2004. High-calcium pyroxene as an indicator of igneous differentiation in asteroids and meteorites. Meteorit. Planet. Sci. 39, 1343–1357.

Sunshine, J.M., Bus, S.J., Corrigan, C.M., McCoy, T.J., Burbine, T.H., 2007. Olivine-dominated asteroids and meteorites: Distinguishing nebular and igneous histories. Meteorit. Planet. Sci. 42, 155–170.

Tanga, P., Cellino, A., Michel, P., Zappalà, V., Paolicchi, P., dell'Oro, A., 1999. On the size distribution of asteroid families: The role of geometry. Icarus 141, 65–78.

USGS, 2006. http://speclab.cr.usgs.gov/spectral-lib.html.

Vokrouhlický, D., Brož, M., Morbidelli, A., Bottke, W.F., Nesvorný, D., Lazzaro, D., Rivkin, A., 2006. Yarkovsky footprints in the Eos family. Icarus 182, 92–117.

Weisberg, M.K., Prinz, M., Kojima, H., Yanai, K., Clayton, R.N., Mayeda, T.K., 1991. The Carlisle Lakes-type chondrites—A new grouplet with high Delta(17)O and evidence for nebular oxidation. Geochim. Cosmochim. Acta 55, 2657–2669.